Mineralium Deposita (2000) 35: 656–671

ARTICLE

H. H. Asadi · J. H. L. Voncken
R. A. Kühnel · M. Hale

Petrography, mineralogy and geochemistry of the Zarshuran Carlin-like gold deposit, northwest Iran

Received: 13 May 1999 / Accepted: 2 February 2000

Abstract Gold mineralisation at Zarshuran, northwestern Iran, is hosted by Precambrian carbonate and black shale formations which have been intruded by a weakly mineralised granitoid. Granitoid intrusion fractured the sedimentary rocks, thereby improving conditions for hydrothermal alteration and mineralisation. Silicification is the principal hydrothermal alteration along with decalcification and argillisation. Three hydrothermal sulphide mineral assemblages have been identified: an early assemblage of pyrrhotite, pyrite and chalcopyrite; then widespread base metal sulphides, lead-sulphosalts and zoned euhedral arsenical pyrite; and finally late network arsenical pyrite, massive and colloform arsenical pyrite, colloform sphalerite, coloradoite, and arsenic–antimony–mercury–thallium-bearing sulphides including orpiment, realgar, stibnite, getchellite, cinnabar, lorandite and a Tl-mineral, probably christite. Most of the gold at Zarshuran is detectable only by quantitative electron microprobe and bulk chemical analyses. Gold occurs mainly in arsenical pyrite and colloform sphalerite as solid solution or as nanometre-sized native gold. Metallic gold is found rarely in hydrothermal quartz and orpiment. Pure microcrystalline orpiment, carbon-rich shale, silicified shale with visible pyrite grains and arsenic minerals contain the highest concentrations of gold. In many ways Zarshuran appears to be similar to the classic Carlin-type sediment-hosted disseminated gold deposits. However, relatively high concentrations of tellurium at Zarshuran, evidenced by the occurrence of coloradoite (HgTe), imply a greater magmatic contribution in the mineralising hydrothermal solutions than is typical of Carlin-type gold deposits.

Editorial handling: L. Miller

H. H. Asadi
Ministry of Culture and Higher Education,
Dr. Beheshti Avenue, Shahid Sabounchi Cross, Tehran, Iran

H. H. Asadi · R. A. Kühnel · M. Hale
International Institute for Aerospace Survey and Earth Sciences,
Kanaalweg 3, 2628 EB Delft, Netherlands

J. H. L. Voncken (✉) · M. Hale
Faculty of Civil Engineering and Geosciences,
Department of Applied Earth Sciences,
Delft University of Technology,
Mijnbouwstraat 120, 2628 RX Delft, The Netherlands
e-mail: j.h.l.voncken@ta.tudelft.nl

Introduction

Zarshuran, located near the town of Takab in northwestern Iran (Fig. 1), is an area of ancient arsenic and gold mining. In modern times, orpiment and realgar have been mined on a small scale for several decades. During the last 10 years, an area of about 1 km^2 around the arsenic mine has been the target of gold exploration. Geological mapping, soil geochemistry, trenching and drilling have been carried out. Results to date indicate a probable reserve of 2.5 million tonnes of ore with an average grade of 10 ppm Au (Samimi 1992).

Scientific knowledge of the Zarshuran deposit is lagging behind its economic evaluation and this may ultimately constrain its commercial development. This paper describes the mineralisation and alteration at Zarshuran and comments on the suitability of applying a Carlin-type model to the deposit.

Methods

Information was taken from the earlier petrographic and mineralogic reports of Bariand (1962), Bariand et al. (1968), Karimi (1993) and Mehrabi et al. (1999) and integrated with observations on 17 thin sections, 5 polished thin sections and 28 polished sections made from samples from tunnels, trenches, boreholes and outcrops at Zarshuran. Descriptions of the hand specimens from which these sections were prepared are given in Table 1. Petrographic and mineralogic examinations were carried out at the Department of Applied Earth Sciences of Delft University of Technology and at the International Institute for Aerospace Survey and Earth Sciences, Delft, The Netherlands.

Petrography was determined by optical examination of thin sections and polished thin sections using transmitted light

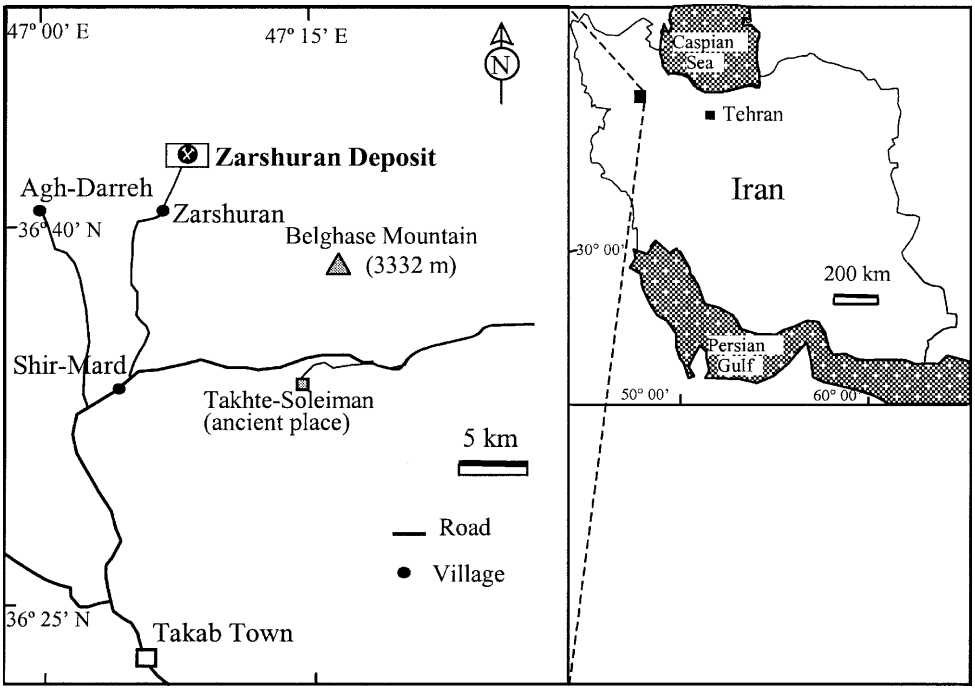

Fig. 1 Location map of Zarshuran deposit in north Takab area, northwest Iran

microscopy, supported by recalculation of the compositions of representative host rock samples determined by total rock analyses by X-ray fluorescence and atomic absorption spectrophotometry, carried out at the Geological Survey, Teplice, Slovakia (Table 2). X-ray diffraction analyses with a Philips PW3710 X'pert system, Cukα X-ray radiation ($\lambda = 1.5418$) and a Ni filter were used to confirm the identity of alteration minerals. A reflected light optical microscope was used for initial examination of polished sections, and polished thin sections and mineral identifications were made with the aid of the so-called Delft System (Kühnel et al. 1980; Glass and Voncken 1996). Qualitative criteria (colour, pleochroism, internal reflection, polishing hardness, shape and form) and estimated quantitative features (anisotropy, reflectance and Vickers microhardness) were used for mineral identification.

The compositions of selected minerals were determined on carbon-coated polished sections using a Jeol electron probe microanalyser (JXA-8800M) in qualitative, quantitative and X-ray scanning modes. The instrument is fitted with three wavelength dispersive spectrometers and with sets of LDE1/TAP and PET/LIF analysing crystals. Standards used for instrument calibration included native gold, iodyrite for silver, galena for lead and sulphur, sphalerite for zinc, marcasite for iron, cinnabar for mercury, a synthetic GaAs (gallium arsenide) compound for arsenic and Sb_2Te_3 for antimony and tellurium. Counting times for the concentrations of major elements were 20 to 50 s using an accelerating voltage of 20 kV and a beam current of 2×10^{-8} A. Analysis for gold was made with a counting time of 300 s on peak and background using an accelerating voltage of 40 kV and a beam current of 4×10^{-8} A, giving a detection limit of about 20 ppm. Details of Au-trace analysis by microprobe can be found in a specialised paper concerning invisible gold in this deposit (Asadi et al. 1999). Atomic concentrations of elements and the number of atoms in the mineral formula were used to determine mineral compositions; computer software calculated the stoichiometry of each mineral.

Geology

The Zarshuran area is underlain mainly by rocks of Precambrian age. The oldest unit, the Iman-Khan schist, forms the core of the Iman-Khan anticline, symmetrically plunging NW–SE over some 6 km. The Iman-Khan schist is followed upwards by the Chaldagh limestone, the Zarshuran black shale, which contains up to 7.38% carbon, and the Qaradash shale, tuff and sandstone. An Oligo-Miocene granitoid, intruded into the mineralised Precambrian formations, is highly altered and mylonitised (Fig. 2).

The lowermost unit in the area, the Iman-Khan schist, is mainly chlorite–amphibole–schist (Table 1; sample 96101) and locally serpentinite (sample 96102). These metamorphic rocks are locally cut by carbonate veins (sample 96100).

The Chaldagh limestone is mainly composed of anhedral to subhedral calcite and dolomite (0.05–0.8 mm). It has a compact mosaic texture and light grey colour imparted by traces of organic matter (sample 96103). The texture is locally laminated due to variations in carbon content. Pyrite, iron oxides, barite and quartz are disseminated in the carbonate matrix. At its base the limestone grades into calc-schist which is strongly mylonitised and shows evidence of hydrothermal mineralisation; calcite and dolomite are partially dissolved and replaced by silica (Fig. 3).

The finely laminated Zarshuran black shale comprises 45–55% calcite, 25–35% quartz (0.1–0.2 mm), 5% dolomite, 5–10% micaceous minerals, $< 3\%$ opaque minerals, mainly pyrite, zircon and rutile, and $\sim 1\%$ detrital potassium feldspar (Fig. 4). The calcite and dolomite are partially replaced by silica. The shale owes its colour to the presence of a substantial amount of organic matter (sample BH1–79). The shale contains jasperoid lenses and dolomitic limestone intercalations in which the dolomite and calcite have a granoblastic texture and which contain minor iron oxides and disseminated opaque minerals such as pyrite, sphalerite and galena (samples BH1–135, BH10–85).

The granitoid dyke or stock contains large phenocrysts of quartz in a white cryptocrystalline groundmass. Its mineral composition is 40–45 vol% quartz (50 μm–8 mm), 10–15 vol% sericitised feldspars (40 μm–0.1 mm) and $< 5\%$ elongated mica and opaque minerals in a matrix of fragmented quartz and sericite (40–45 vol%). On the basis of the fragmented nature of much of the quartz, its very strong undulous/wavy extinction (Fig. 5) and its close contact with some of the sericitised feldspar, the granitoid can be described as a mylonite or an ultramylonite. Analysis by X-ray diffraction revealed the presence of kaolinite and qualitative electron microprobe analyses revealed the presence of pyrite, cinnabar, iron oxides, mica and accessory minerals such as zircon, apatite and xenotime, some of which occur within very small fractures in sericite. Whole rock

Table 1 Descriptions of the samples used for chemical analysis, and petrographic and mineralogic studies

Sample no.	Rock type/mineral	Location	Remarks
96100	Calcite	50 m to the north of mine valley	Thin calcitic veins cutting Iman-Khan schist
96101	Iman-Khan metamorphic rocks	50 m to the north of mine valley	Green schist, basement rock, core of Iman-Khan anticline
96102	Iman-Khan metamorphic rocks	200 m to the north of mine office	–
96103	Chaldagh limestone	250 m northwest of mine office	Light grey crystalline limestone with compact texture
96104	Mylonitised Chaldagh limestone	Southeast of mine valley, close to the Tunnel 9	Brittle limestone collected at the lower contact with the basement schist
96105	Zarshuran black shale	Karbelai-Abbas valley	Finely laminated carbon-rich shale
96106	Jasperoid	25 m to the northwest of mine office	Unmineralised carbon-poor jasperoid with grey-white colour
96107	Jasperoid	150 m to the northwest of mine office	Unmineralised carbon-poor jasperoid with grey-white colour
96108, 96109	Altered granitoid	Southeast of mine valley, near the borehole no. 1	White rock containing large phenocrysts of quartz
96110	Powdery Chaldagh limestone	Southeast of mine valley, above the Tunnel 8	Sample collected on a fault zone at the upper contact with Zarshuran Unit
96111	Alteration	Tunnel 8	Spare zones within the Zarshuran Unit
96112	Quartz veins	250 m to the northwest of mine office	Quartz veins containing barite and calcite located in the Chaldagh limestone
96113	Oxidised quartz vein	Trench in Karbelai-Abbas valley	Fe oxides are abundant in this rock
96114	Jasperoids	Tunnel 8	Mineralised quartz veins
96115	Jasperoids	Tunnel 8	Visible sphalerite and fluorite in hand specimen
96116	Altered granitoid	Southeast of mine valley	White rock with large quartz phenocrysts
96117	Quartz with orpiment	Tunnel 8	Mineralised rock
96118	Dense microcrystalline arsenic minerals	Tunnel 8	Arsenic ore with high gold content
96119	Crystalline arsenic mineral	Tunnel 8	Arsenic ore
96120	Carbon-rich quartz veins	Tunnel 9	Carbonaceous ore with high gold content
96121	Carbon-rich quartz veins	Tunnel 9	Carbonaceous ore with high gold content
96122	Carbon-rich quartz veins with arsenic minerals	Tunnel 8	Carbonaceous and arsenic ore
97201	Altered granitoid	Karbelai-Abbas valley	White rock with large quartz phenocrysts
97202	Quartz veins	Tunnel 8	Mineralised rock
97203	Black shale	Tunnel 8	Mineralised black shale with getchellite
97204	Quartz veins	TR2 trench, west of Karbelai-Abbas valley	Minerals are crystalline quartz, calcite and orpiment
97205	Quartz and pyrite	Tunnel 8	Visible pyrite grains taken from quartz veins
BH8–160	Mineralised limestone	160 m depth in borehole no. 8	Brittle limestone with visible pyrite grains (chemical analysis shows 20 ppm Au)
BH1–79	Black shale	79 m depth in borehole no. 1	Finely laminated carbon-rich shale (carbonaceous ore)
BH1–135	Limestone	135 m depth in borehole no. 10	Limestone intercalations in Zarshuran Unit
BH10–85	Limestone and As minerals	85 m depth in borehole no. 10	Mineralised sample

analysis showed an average of 77.36% SiO_2, 16.1% Al_2O_3, 2.23% K_2O, 1.24% (Fe_2O_3 + FeO) and 1.1% CaO (samples 96108, 96116, Table 2). The mineralogic and geochemical data suggest that the parent granitoid was probably a quartz porphyry.

Mineralisation

Mineralisation at Zarshuran occurs in the Zarshuran black shale and Chaldagh limestone, extending in a north-northwest direction over some 5–6 km along the southeastern flank of the Iman-Khan anticline. The highly mineralised zone, which extends over about 1 km, dips approximately 45° to the southwest and is intersected by two sets of high-angle faults trending NW–SE and E–W (Fig. 2). The Iman-Khan schist is only weakly mineralised over a few metres at its upper contact with the Chaldagh limestone. In the Chaldagh limestone gold is concentrated in quartz veins up to 3 m wide and cross-cutting veinlets that occur throughout the Chaldagh limestone. Also, the limestone contains disseminated mineralisation over about 10 m at its lower contact with the schist and at its upper contact with the Zarshuran unit. Gold is disseminated through the 5–75-m-thick Zarshuran black shale, with the richest mineralisation occurring in the calcareous, carbonaceous and siliceous intercalations and veins.

Mineralisation is accompanied by silicification. Quartz veins occupying the NW–SE and E–W high-

Table 2 Total analysis and trace element analysis of representative host rocks at Zarshuran (in wt%, except as stated). *nd* Not determined

Sample no.	96103	BH 1–135	BH 1–79	96114	96108	96116
SiO_2	0.69	1.76	36.60	91.8	76.11	78.62
CaO	54.15	53.32	25.40	0.35	1.48	0.67
Al_2O_3	0.21	0.34	5.65	2.3	17.10	15.06
Fe_2O_3, FeO	0.28	0.84	4.16	0.85	1.16	1.32
MgO	0.47	0.56	0.97	0.06	0.24	0.30
Na_2O	0.02	0.04	0.06	0.01	0.2	0.06
K_2O	0.04	0.06	1.41	0.30	2.26	2.19
MnO	0.002	0.071	0.118	0.02	0.083	0.055
TiO_2	0.01	0.02	0.77	0.02	0.14	0.24
P_2O_5	0.03	0.02	0.06	0.12	0.37	0.42
SO_3	0.03	0.05	0.38	0.25	0.16	0.22
CO_2	43.65	42.46	23.35	0.16	0.53	0.20
Total	100.01	100.10	100.45	100.09	100.15	100.14
Trace element analysis						
Au (ppm)	0.16	0.36	9.57	2.42	0.15	0.14
As	0.25	0.12	0.06	3.22	0.08	0.04
Ag (ppm)	< 0.2	0.2	0.4	3.2	0.25	0.2
Sb	0.002	0.032	0.007	0.029	0.004	0.003
Te (ppm)	< 0.5	1.0	< 0.5	18.1	< 0.5	< 0.5
Tl (ppm)	1.3	1.6	20.5	8.0	2.3	1.4
Hg (ppm)	4.45	4.53	26.14	62.6	5.2	3.060
Zn	0.272	0.1	0.055	0.103	0.05	0.064
C	nd	nd	7.38	1.84	nd	nd
S	0.46	0.61	1.91	4.9	0.85	0.63

angle faults cut the mineralised formations, and quartz partially replaces carbonates. The quartz veins in the Chaldagh limestone contain cross-cutting barite and microscopic pyrite, arsenical pyrite, sphalerite and iron oxides (sample 96112). The mineralised quartz veins and jasperoid lenses in the Zarshuran black shale contain arsenic–antimony sulphides, pyrite, arsenical pyrite, base metal sulphides, lead-sulphosalts, barite, fluorite and iron oxides. The altered granitoid is weakly mineralised and closely associated with the mineralised jasperoid lenses in the Zarshuran black shale.

About 30 sulphide minerals and sulphosalts have now been identified at Zarshuran. Those recognised by Bariand (1962), Bariand et al. (1968), Karimi (1993) and Mehrabi et al. (1999) are included in Table 3, along with those now identified for the first time and described below.

Pyrite is one of the most abundant sulphides associated with ore and gangue minerals in the Zarshuran black shale and the Chaldagh limestone. Both diagenetic and hydrothermal pyrites are present. Diagenetic pyrites lack gold and arsenic in their composition, and occur as euhedral to subhedral crystals (< 0.1 mm), mainly along the bedding planes in the Zarshuran black shale unit, and as minor framboidal aggregates typically a few micrometres, but in some cases up to several tens of micrometres in diameter. In the unmineralised parts of

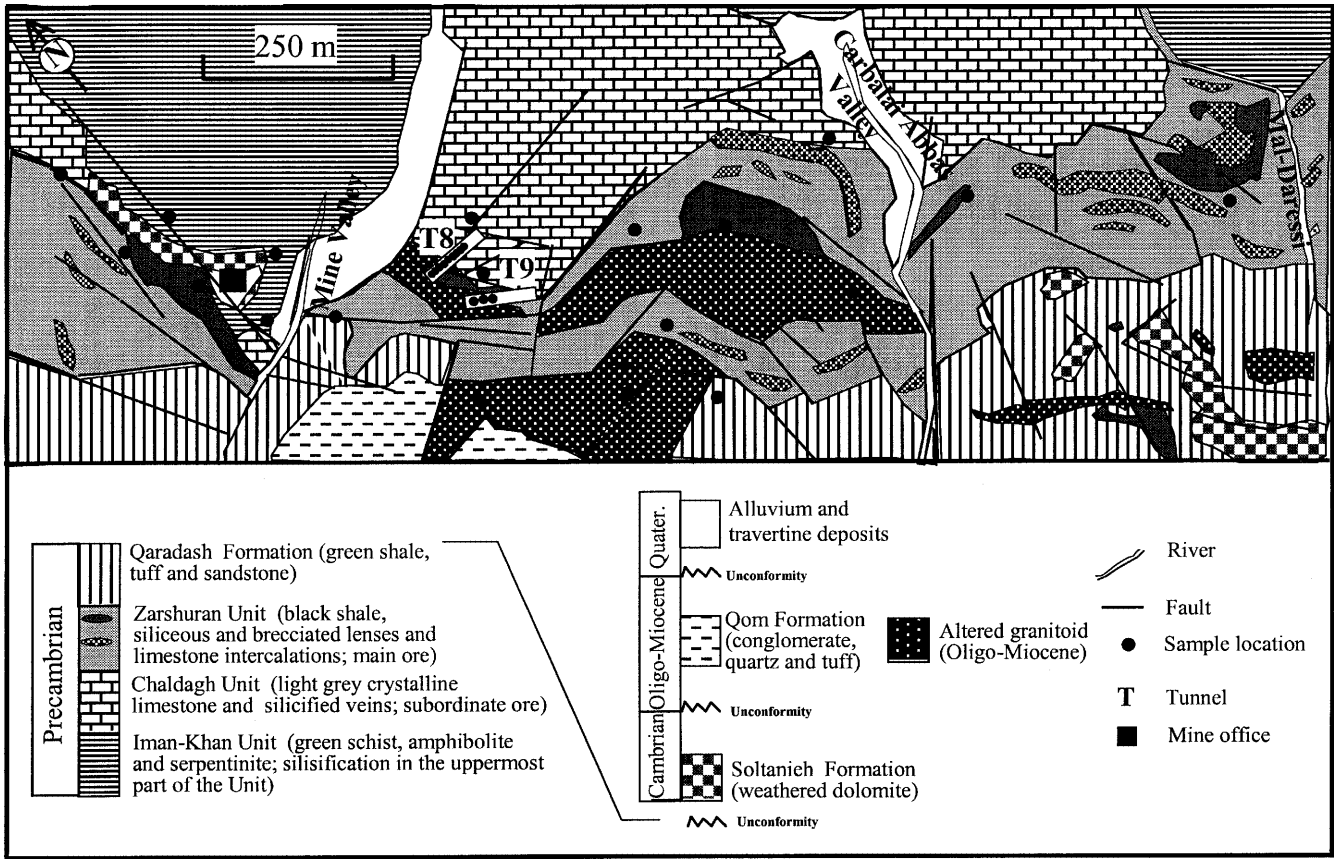

Fig. 2 Geology of the Zarshuran deposit. (Modified after Ojaghi 1995)

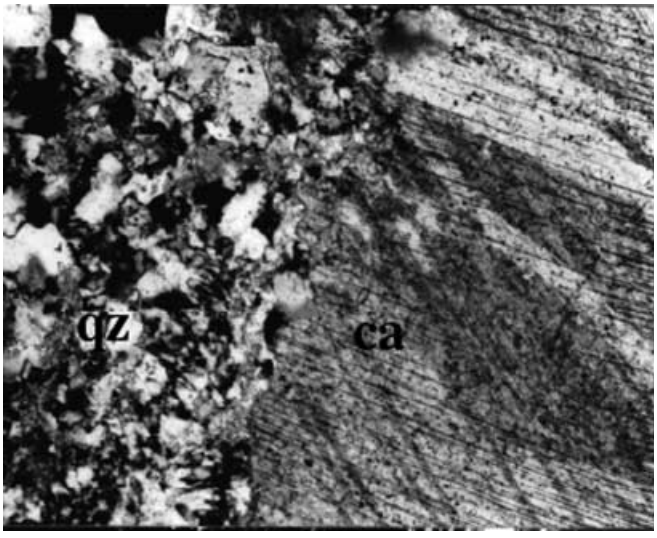

Fig. 3 Photograph of Chaldagh limestone (*ca* calcite) replaced by hydrothermal quartz (*qz*); sample 96104. Width of the picture is 0.35 mm

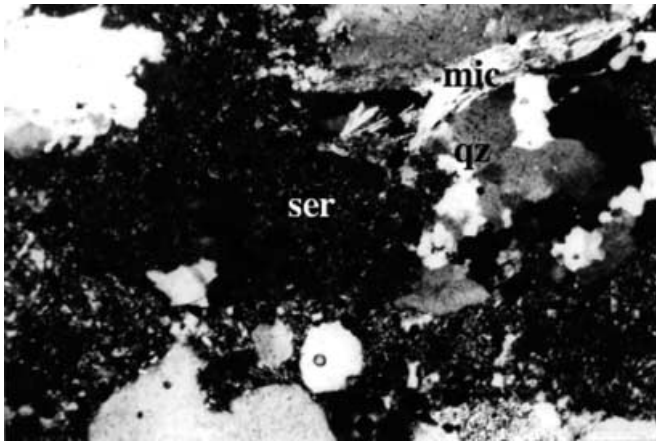

Fig. 5 Strongly altered granitoid rock with quartz (*qz*) showing undulatory extinction, sericite matrix (*ser*) and elongated mica (*mic*); sample 96109. Width of the photograph is 0.55 mm

the Chaldagh limestone, diagenetic pyrite occurs mainly as isolated framboidal aggregates and as disseminated crystals of ~5 μm in size.

In the mineralised parts of the Zarshuran and Chaldagh formations, hydrothermal pyrite has different modes of occurrence. Pyrite that is anhedral is relatively pure and in some cases has inclusions of pyrrhotite (Karimi 1993). However, the principal mode of occurrence is disseminated euhedral to subhedral crystals in quartz (Fig. 6a) and, less commonly, in fluorite, barite, calcite, sphalerite, and arsenic and antimony minerals. High-resolution optical microscopy and electron microprobe analyses show that some of the large grains of euhedral pyrite (5–300 μm) have a zoning of arsenic, mercury, antimony and gold (Fig. 6b, c). An arsenic-rich zone (up to 6.5% As) appears brighter on a back-scattered image than pyrite of low arsenic content (Fig. 6d, e). Often surrounding zoned pyrite are network and massive arsenical pyrite, which are considered to be late hydrothermal pyrites. Some pyrite has a colloform texture and contains up to 4.5% As (Fig. 6f). This colloform arsenical pyrite is intimately intergrown with massive and colloform sphalerite. The arsenical pyrites are directly associated with gold mineralisation (Asadi et al. 1999).

In altered granitoid, hydrothermal pyrite occurs as very fine grains (< 1 μm) precipitated along the quartz grain boundaries, in fractures in quartz and on the surfaces of clay minerals (Fig. 7a). The pyrite precipitated along the quartz grain boundaries has the appearance of veinlets when viewed at low magnification. This pyrite occurs in close association with grains of cinnabar.

Anhedral grains of marcasite (20–50 μm) occur in minor quantities in close association with pyrite in the

Fig. 4 Photographs of black shale: **a** angular quartz grains (*qz, bright*), calcite (*ca, white-grey*) and hydrocarbons (*org, dark seams*); **b** concentration of quartz grains and flooding of hydrocarbons along bedding; sample BH1–79. Width of each photograph is 0.35 mm

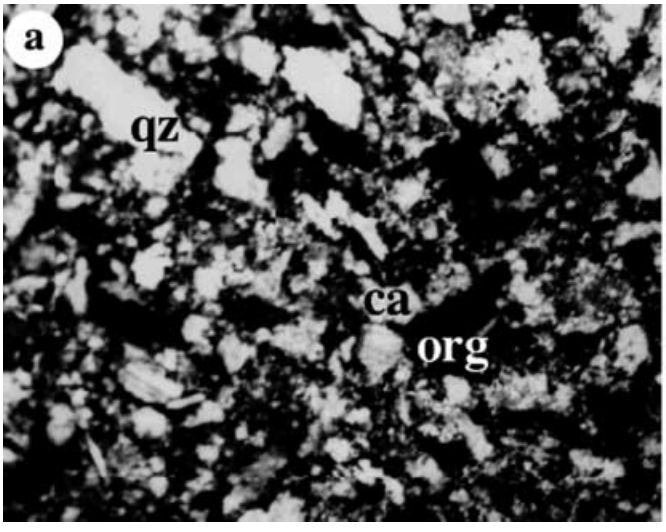

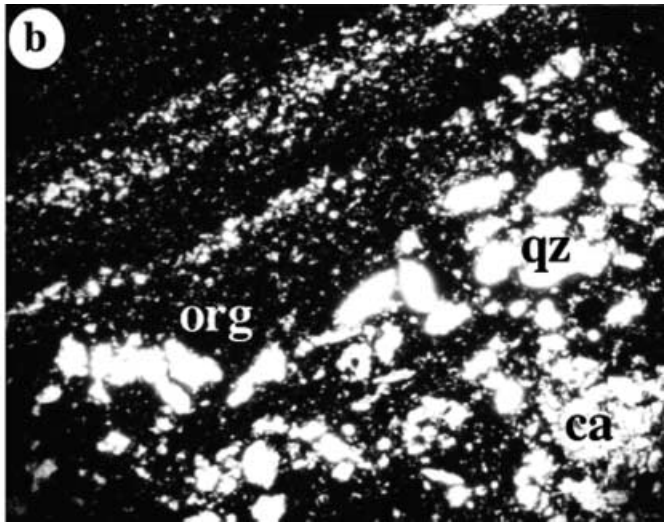

Table 3 Alphabetic list of minerals identified so far in the Zarshuran gold deposit

Mineral	Composition	Reference[a]	Method[b]	Abundance[c]
Aktashite[d]	$Cu_6Hg_3As_4S_{12}$	4	EPMA	R
Apatite	$Ca_5(PO_4)_3(OH,F,Cl)$	1,3,4	EPMA	R
As/Sb oxides	As_2O_3, Sb_2O_3	1,2,4	EPMA	R
Barite	$BaSO_4$	1,2,3,4	EPMA, M	C
Baumhauerite[d]	$Pb_3(As)_4S_9$	4	EPMA	R
Boulangerite[d]	$8[Pb_5Sb_4S_{11}]$	1,2,4	Re	R
Calcite	$CaCO_3$	1,2,3,4	EPMA, M, F	C
Chalcopyrite	$CuFeS_2$	1,2,3,4	M	R
Christite (uncertain)	$TlHgAsS_3$	4	EPMA	R
Cinnabar	HgS	1,2,3,4	EPMA, M	R
Coloradoite	HgTe	4	EPMA, M	R
Covellite	CuS	1,3	Re	R
Dolomite	$(Ca,Mg)CO_3$	1,2,3,4	M, EPMA	C
Fluorite	CaF_2	1,2,3,4	EPMA, M	A
Galena	PbS	1,2,3,4	EMPA, M	R–S
Galkhaite	$[(Hg,Cu,Zn,Tl,Fe)_6$ $(Cs,Tl)\ (As,Sb)_4S_{12}]$	3	Re	R
Geocronite[d]	$Pb_5\ (As,\ Sb)_2S_8$	1,3,4	EPMA, M	R
Getchellite	$AsSbS_3$	1,2,3,4	EPMA, M	R
Goethite	FeO(OH)	1,2,3,4	F	C
Gold	Au	2,3,4	EPMA, M	R
Gypsum	$CaSO_4{\cdot}2H_2O$	1,2,3,4	F	C
Illite	$KAl_4\ [Si_4\ O_{10}](OH)$	1,2,3,4	XRD	–
Jarosite	$KFe_3(SO_4)_2(OH)_6$	1,2	Re	–
Kaolinite	$Al_4[Si_4O_{10}](OH)$	1,2,3,4	XRD	C
Kermesite	Sb_2S_2O	1,2	Re	–
K-feldspar	$KAlSi_3O_8$	1,2,3,4	EPMA, M	C
Lautite	(Cu, As, Fe)S	3	Re	R
Limonite	$FeO(OH){\cdot}nH_2O$	1,2,3,4	F	C
Lorandite	$TlAsS_2$	1,2,3,4	XRD	R
Marcasite	FeS_2	1,2,3,4	M	R
Melnikovite	FeS1–2	1,2,4	EPMA, M	R
Metacinnabar	(HgFeZn)S	1	Re	–
Orpiment	As_2S_3	1,2,3,4	EPMA, M	A
Plagionite[d]	$Pb_5Sb_8S_{17}$	4	EPMA	R
Pyrite	FeS_2	1,2,3,4	EMPA, M	A
Pyrrhotite	$Fe_{1-x}S$	1,2	Re	R
Quartz	SiO_2	1,2,3,4	EPMA, M	C
Realgar	AsS	1,2,3,4	EPMA, M	S
Rutile	TiO_2	1,3,4	EPMA	R
Scorodite	$(Fe,\ As)O_4{\cdot}2H_2O$	1,2,3	Re	–
Semseyite[d]	$(Pb_9Sb_8S_{21})$	4	EPMA	R
Sericite	$K_2Al_4[Si_6Al_2O_{20}](OHF)_4$	1,2,3,4	M	C
Simonite	$(TlHgAs_3S_6)$	3	Re	R
Sphalerite	ZnS	1,2,3,4	EPMA, M	S
Stibnite	Sb_2S_3	1,2,3,4	EPMA, M	S
Twinnite[d]	$Pb(As,Sb)_2S_4$	4	EPMA	R
Xenotime	YPO_4	3,4	EPMA	R
Zircon	$ZrSiO_4$	3,4	EPMA	R

[a] *1* Bariand (1962), Bariand et al. (1968), *2* Karimi (1993), *3* Mehrabi et al. (1999) and *4* present study
[b] *EPMA* Electron probe micro analysis, *M* polarising microscope, *F* field observation, *XRD* X-ray diffraction, *Re* reported
[c] *C* Common, *A* abundant, *S* subordinate, *R* rare
[d] Mineral phase discussed in a separate paper

mineralised black shale. Although Oberthur et al. (1997) interpret marcasite as a primary constituent of ores precipitated during the waning stages of hydrothermal mineralisation, its mode of occurrence and interrelations at Zarshuran suggest that it is a supergene alteration product replacing pyrite.

Sphalerite is the most abundant base metal sulphide. It occurs in jasperoids and black shale in one of two habits. Anhedral grains (< 1 mm), intimately intergrown with galena (Fig. 7b) and lead-sulphosalts, are found in association with pyrite; in places pyrite inclusions (2–3 μm) occur in sphalerite. Massive and colloform sphalerite is associated with quartz, orpiment, stibnite and colloform arsenical pyrite, and less commonly with carbonate, barite and fluorite (Figs. 6f and 7c). Electron microprobe analyses indicate substantial amounts of gold in colloform sphalerite (Asadi et al. 1999).

Other base metal sulphides at Zarshuran are galena and chalcopyrite. Galena is rare and often intergrown with sphalerite (Fig. 7b), closely associated with

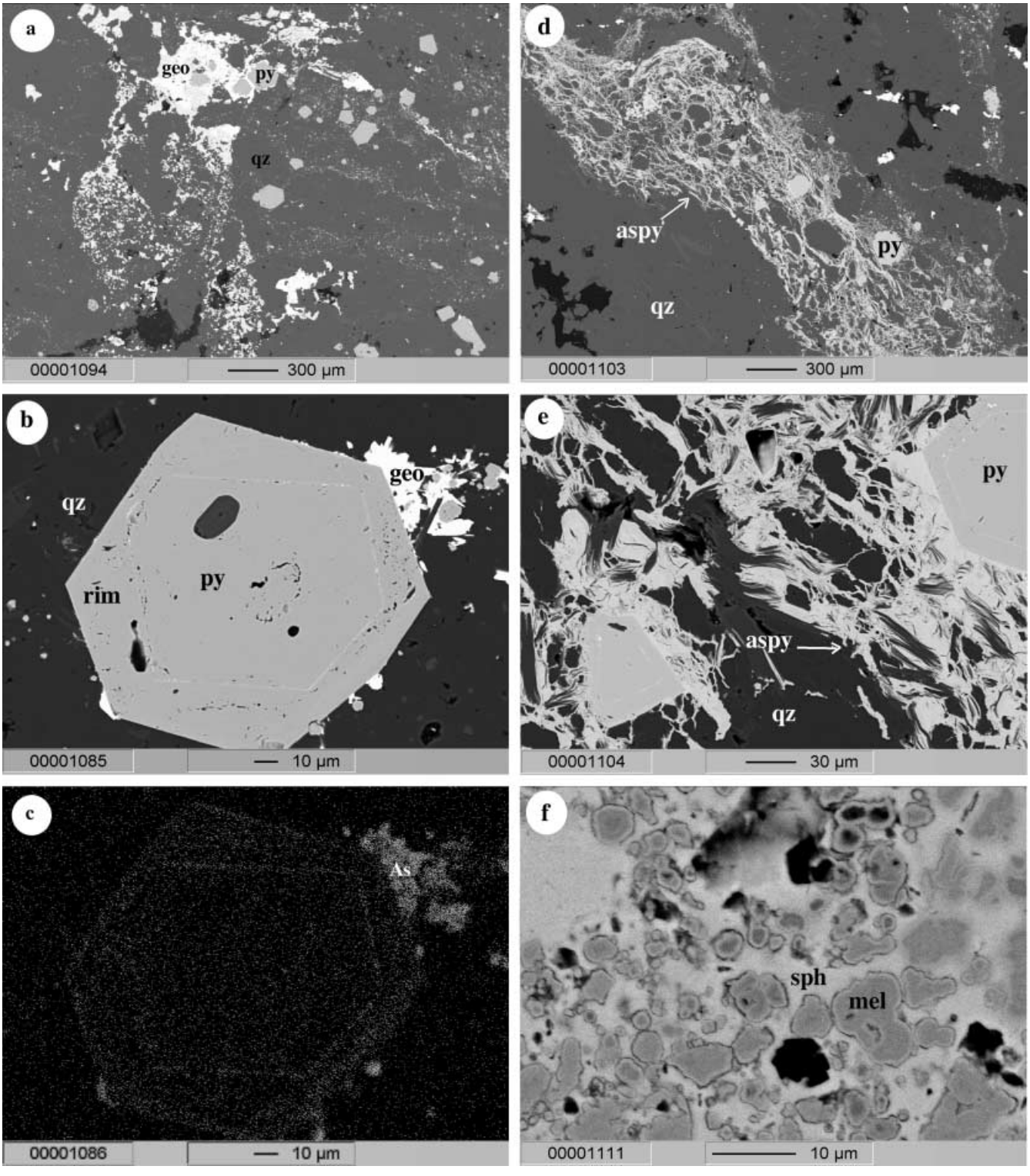

Fig. 6 Back-scattered electron micrographs of pyrite and arsenical pyrite in the quartz matrix: **a** overview of disseminated pyrite (*py, light grey*), replaced by geocronite (*geo, white*); **b** detailed disseminated pyrite showing zoned texture, white mineral around the pyrite is geocronite (*geo*); **c** X-ray image of zoned pyrite showing the As concentration in bright colour; **d** overview of network arsenical pyrite (*aspy*); **e** detail of network arsenical pyrite and zoned pyrite; **f** colloform arsenical pyrite or melnicovite (*mel, grey*) surrounded by massive sphalerite (*sph, white-grey*). Samples 96117, 96115 and 96114

lead-sulphosalts and pyrite within a quartz matrix. It occurs in patches, as subhedral and anhedral grains (20–300 µm). Pyrite inclusions (2–3 µm) are occasionally observed in galena. Chalcopyrite is also rare but occurs as a few anhedral crystals (10–250 µm) in close association with pyrite in silicified rocks.

Orpiment (As_2S_3) is the most abundant sulphide at Zarshuran and the main arsenic ore mineral. It occurs in

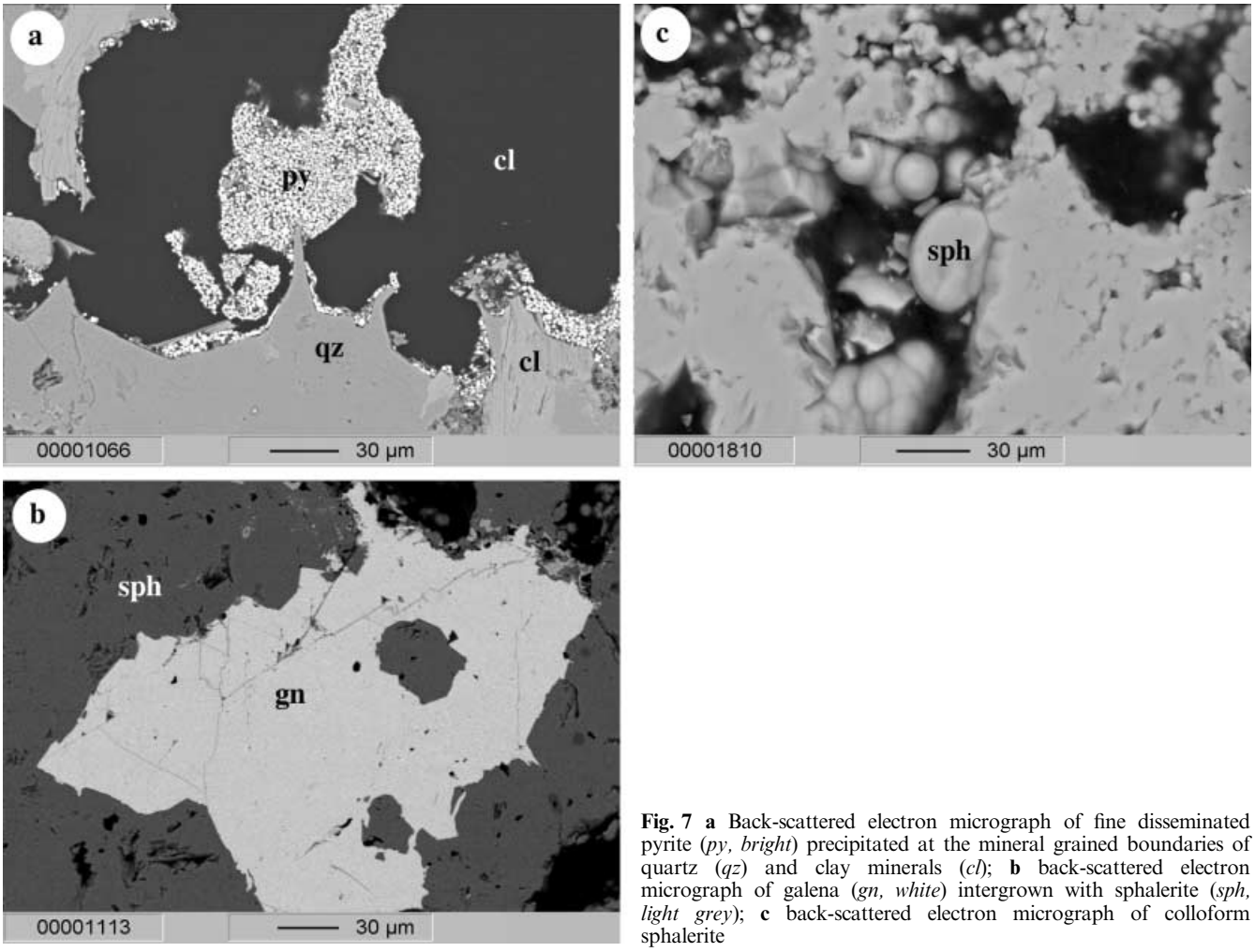

Fig. 7 **a** Back-scattered electron micrograph of fine disseminated pyrite (*py, bright*) precipitated at the mineral grained boundaries of quartz (*qz*) and clay minerals (*cl*); **b** back-scattered electron micrograph of galena (*gn, white*) intergrown with sphalerite (*sph, light grey*); **c** back-scattered electron micrograph of colloform sphalerite

small veins, veinlets, fracture fillings and lenses (up to 3 m) within silicified black shale as massive and coarsely crystalline aggregates of flaky crystals which are randomly oriented and partly deformed (Fig. 8a). The orpiment typically contains antimony and tellurium (Fig. 8b, c; Table 4); electron microprobe analyses revealed up to 0.24% Te and 9% Sb. Antimony probably substitutes for arsenic (Radtke et al. 1973; Dickson et al. 1974). Massive orpiment contains inclusions of pyrite, thallium-bearing minerals, stibnite (Fig. 8e) and minute grains of metallic gold which can be seen by optical microscopy (Fig. 9) but remain undetected by quantitative electron microprobe analyses with a 20 ppm detection limit. Coarsely crystalline orpiment has inclusions of coloradoite aggregates and anhedral arsenical pyrite. Many of the other ore minerals are commonly associated with orpiment.

Realgar (AsS) is a subordinate arsenic mineral ($< 5\%$), occurring as anhedral crystals associated with orpiment, from which it can be differentiated by slightly lower reflectance, more pronounced bi-reflectance, greyer colour and intense red internal reflections. Realgar crystals in the Zarshuran black shale are often deformed (Fig. 8d). They contain traces of tellurium but, compared with orpiment, little antimony (Table 4).

Stibnite (Sb_2S_3) is found as irregular grains, needles (< 50 µm) and needle-shaped aggregates within the orpiment matrix and is in places replaced by massive orpiment (Fig. 8e, f). It also occurs as inclusions in orpiment, getchellite and sphalerite. Inclusions of pyrite and sphalerite are found within stibnite aggregates. Electron microprobe analyses of stibnite grains yielded an average of 3.97 wt% As, probably precipitated as solid solution (Dickson et al. 1974) or present as very fine grains of arsenic minerals (Table 4).

Rare getchellite ($AsSbS_3$) is closely associated with quartz, carbonate, stibnite and twinnite (Table 4). Inclusions of pyrite and fine lamellae of twinnite are found in the matrix of deformed getchellite (Fig. 10a) and elongated crystals of getchellite intersect the dark grey solicited limestone host rock (Fig. 10b). Getchellite is formed when the arsenic–antimony ratio in the hydrothermal solution reaches 1:1 (Bariand et al. 1968).

Lorandite ($TlAsS_2$) was detected by X-ray diffraction analysis of massive orpiment. Another thallium-bearing mineral, suspected to be christite, ($TlHgAsS_3$) was observed (by back-scattered electron imagery) in massive

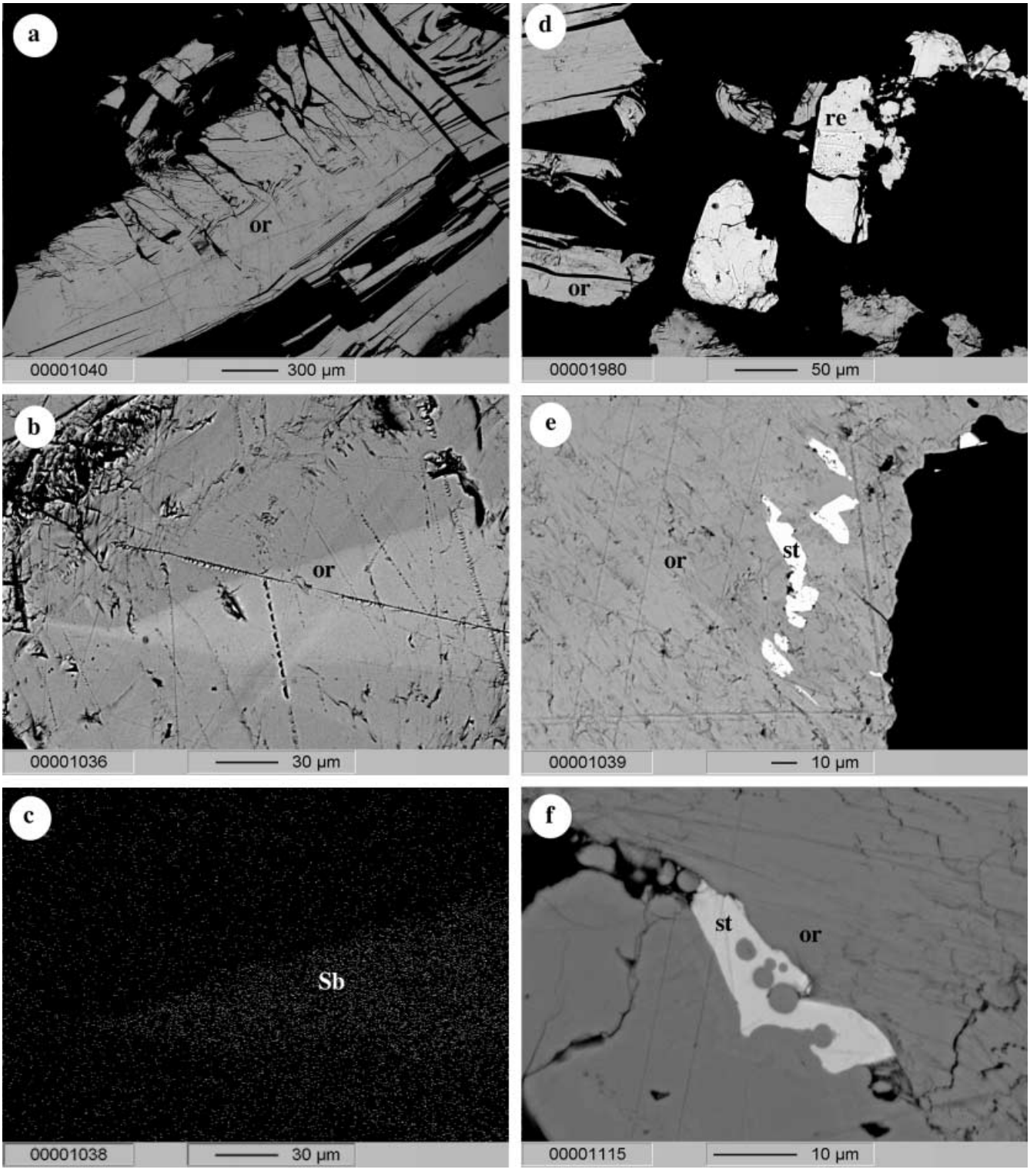

Fig. 8 Back-scattered electron micrographs of orpiment, realgar and stibnite: **a** deformed orpiment crystal (*or, grey*); **b** massive microcrystalline orpiment, bright zone contains higher Sb as shown on X-ray image (map **c**); **d** realgar aggregates occurring with orpiment in the carbon-rich quartz matrix; **e** stibnite grains (*st, white*) occurring in microcrystalline orpiment; **f** detailed stibnite (*st, white-grey*) replaced by orpiment. Samples 96118, 96119 and BH1–79

orpiment as bright needle-shaped inclusions, too small (< 5 µm) to be analysed quantitatively (Fig. 11). The X-ray images and spectrum of this mineral are presumed to correspond with those of christite. Christite is a very rare mineral, and was first recognised at the Carlin gold deposit (Radtke et al. 1977).

Table 4 Average microprobe analysis (wt%) in orpiment, realgar, stibnite and getchellite minerals showing As/Sb variations and Te content. *N* Number of analyses

Mineral	As	Sb	S	Te (ppm)	Total	N	Empirical formula
Orpiment	57.25	4.71	38.70	870[a]	100.66	16	$As_{1.94}$ $Sb_{0.12}$ $S_{2.98}$
Realgar	71.97	0.004	27.81	133	99.80	3	$As_{1.02}$ $S_{0.98}$
Stibnite	3.97	67.57	29.07	0	100.61	4	$Sb_{1.84}$ $As_{0.17}$ $S_{2.95}$
Getchellite	24.141	42.43	33.07	0	99.64	4	$As_{0.98}$ $Sb_{0.99}$ $S_{3.03}$

[a] $N = 13$

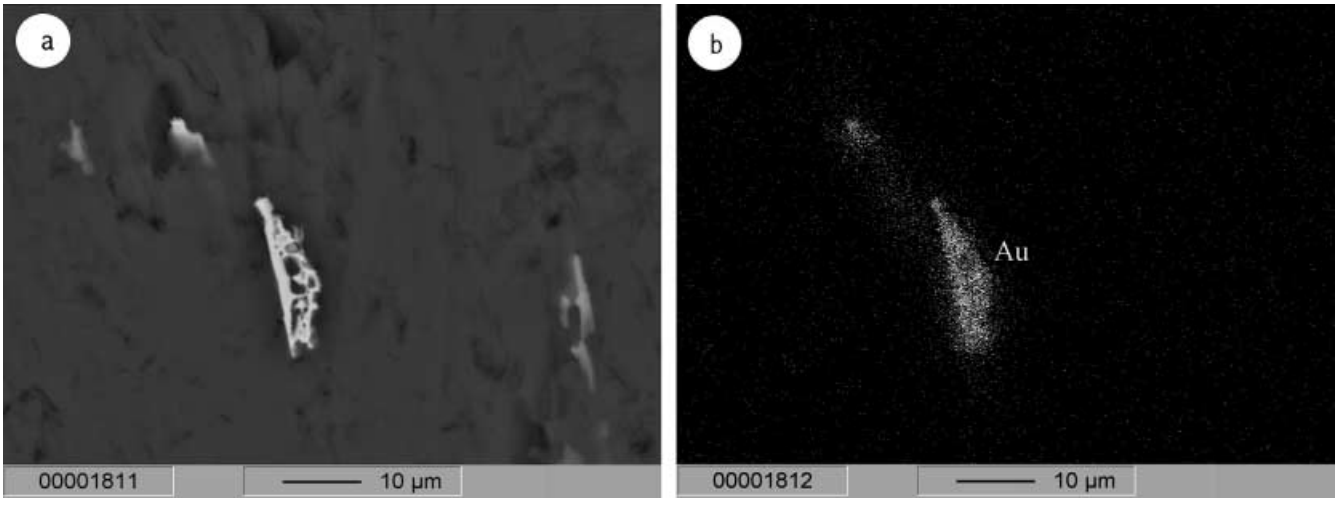

Fig. 9 Scarce native gold at Zarshuran: **a** back-scattered electron micrograph of dendritic gold grain in microcrystalline orpiment matrix; and **b** corresponding X-ray image showing Au concentration

Cinnabar is a minor mineral at Zarshuran, mainly encountered in the highly altered and mylonitised granitoid. Trails of cinnabar inclusions (< 2 µm) and anhedral grains (< 15 µm) are located along quartz grain boundaries and in close association with argillic alteration (Fig. 12). Karimi (1993) mentions metallic gold in cinnabar at Zarshuran, but microprobe analyses of several cinnabar grains failed to confirm this.

Coloradoite (HgTe) is the only telluride so far identified at Zarshuran (Table 5). It is found as rare patches of fine diamond-like grains (< 50 µm) in coarsely crystalline orpiment (Fig. 13a, b).

Alteration

Three types of hydrothermal alteration have been identified at Zarshuran: decalcification, silicification and argillisation. There has also been a late oxidation and acid leaching event.

Fig. 10 **a** Back-scattered electron micrograph of elongated and foliated getchellite (*get, white*) intersecting the carbonate minerals; **b** needle inclusions and lamellas of twinnite occurring in getchellite Sample 97203

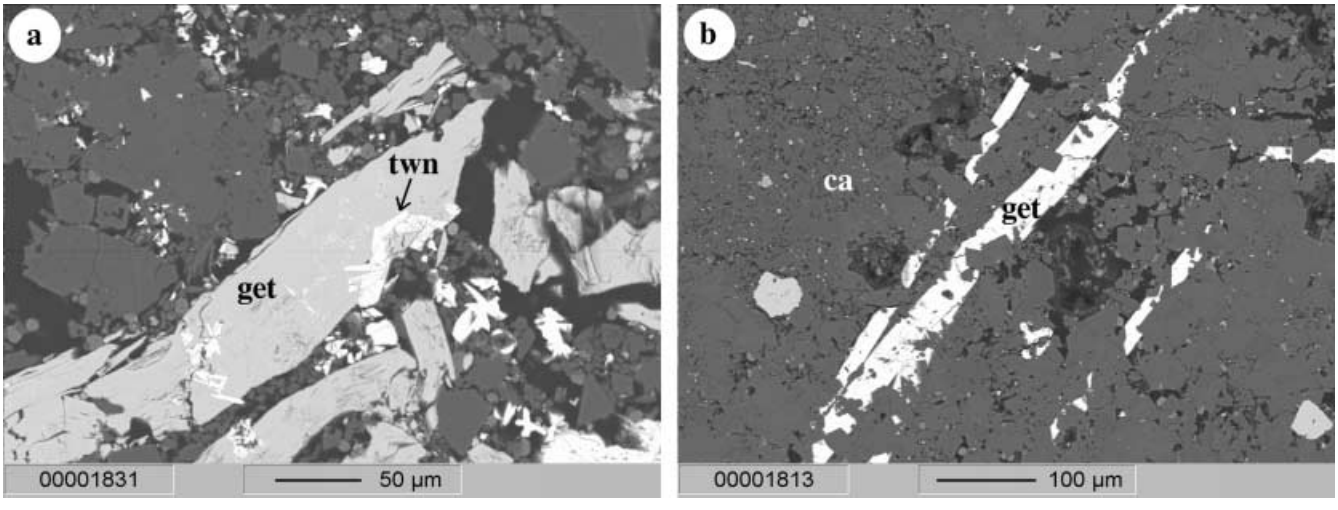

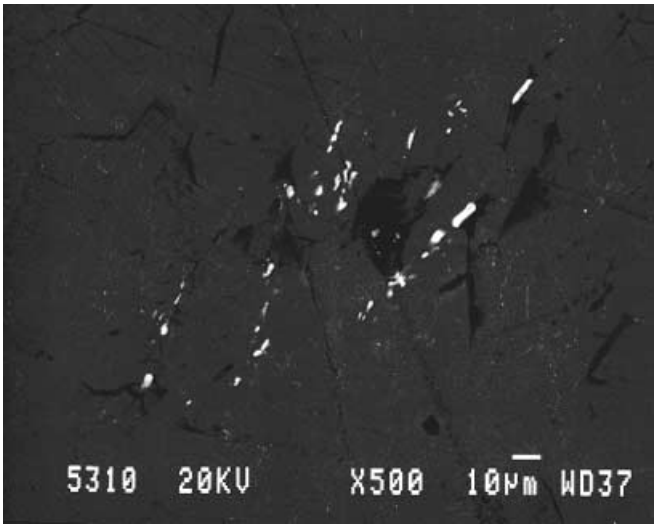

Fig. 11 Back-scattered electron micrograph of oriented needles of the mineral assumed to be christite (*bright needles*) occurring in orpiment matrix. Sample 96118

The calcite and dolomite in both black shale and limestone intercalations are replaced to varying degrees by hydrothermal silica, in extreme cases forming jasperoid with up to 95 vol% of cryptocrystalline quartz. Unmineralised jasperoids occur as white siliceous lenses (samples 96106, 96107) and mineralised jasperoids occur as grey siliceous lenses and veins (samples 96114, 96117, 96120, 96121, 96122, 97202, 97204, 97205).

Decalcification, a partial replacement of carbonate by silica, is conspicuous in a fault zone at the contact of the Chaldagh limestone and Zarshuran black shale, where a powdery limestone has been formed (sample 96110). It is also found in the carbonate horizons of the black shale.

Silicification is the most widespread alteration at Zarshuran and is attributed to neutralisation of acidic silica-rich solutions by carbonates accompanied by precipitation of silica in voids; subsequently the precipitated silica recrystallised into chalcedony and quartz. The intensity of silicification varies from weak to the total replacement of the original rock by jasperoid. It is best developed in the Zarshuran black shale, where there are jasperoid veins and lenses. The Chaldagh limestone is locally silicified along faults and fractures. Highly altered granitoid and carbonate at the contact of the Chaldagh limestone and Zarshuran black shale, and near an E–W trending fault, also shows a siliceous alteration. Massive cryptocrystalline quartz and hydrothermal quartz with idiomorphic hexagonal crystals (1–500 µm) are the main components of siliceous alteration, and are visible on most of the polished and thin sections from silicified zones of the Zarshuran black shale. Two generations of silicification can be recognised: an early, massive silicification with which no

Fig. 12 **a** Back-scattered electron micrograph of accumulation of fine inclusions (*cin, bright*) and trails of cinnabar (*cin trails, bright*) precipitated along the mineral grained boundaries of quartz (*qz, grey*) and clay minerals (*cl, dark grey*, *light grey*); **b** corresponding X-ray image showing the Hg concentration in cinnabar. Sample 97201

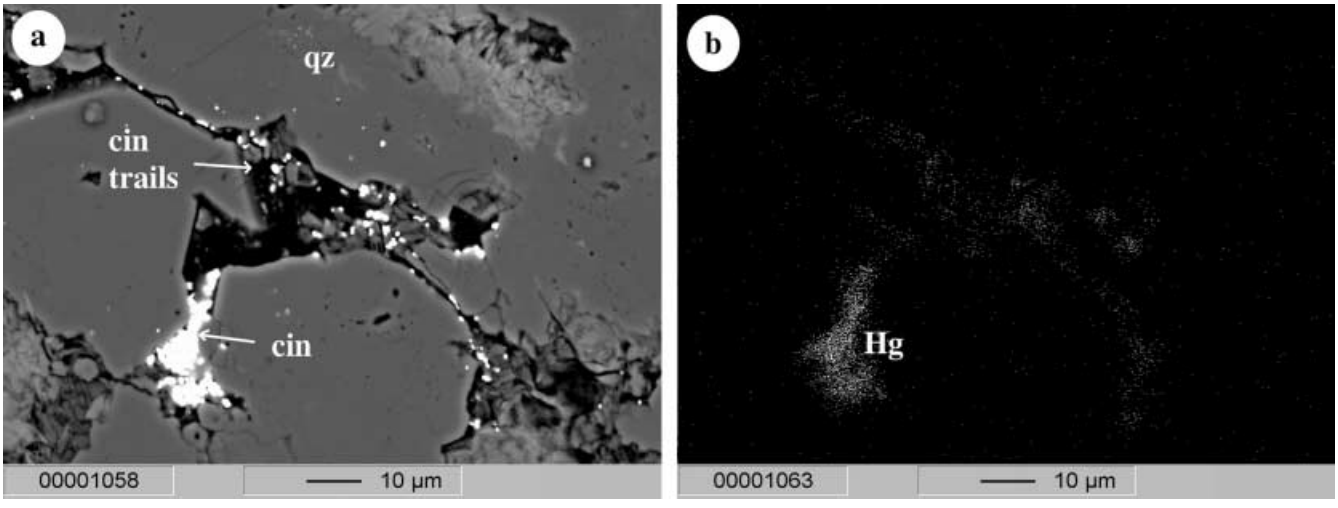

Table 5 Stoichiometry of coloradrfoite. Average analytical formula: $Hg_{0.99}Te_{1.01}$. Ideal formula: HgTe

	Analysis 1 (atom%)	Analysis 2 (atom%)	Analysis 3 (atom%)	Analysis 4 (atom%)	Analysis 5 (atom%)	Average (atom%)
Hg	49.41	49.27	49.23	49.00	48.65	49.11
Te	49.93	50.08	50.03	50.31	50.46	50.16
Total	99.34	99.35	99.25	99.31	99.11	99.27
No. atoms in formula	2	2	2	2	2	2
Hg	0.99	0.99	0.99	0.99	0.98	0.99
Te	1.01	1.01	1.01	1.01	1.02	1.01

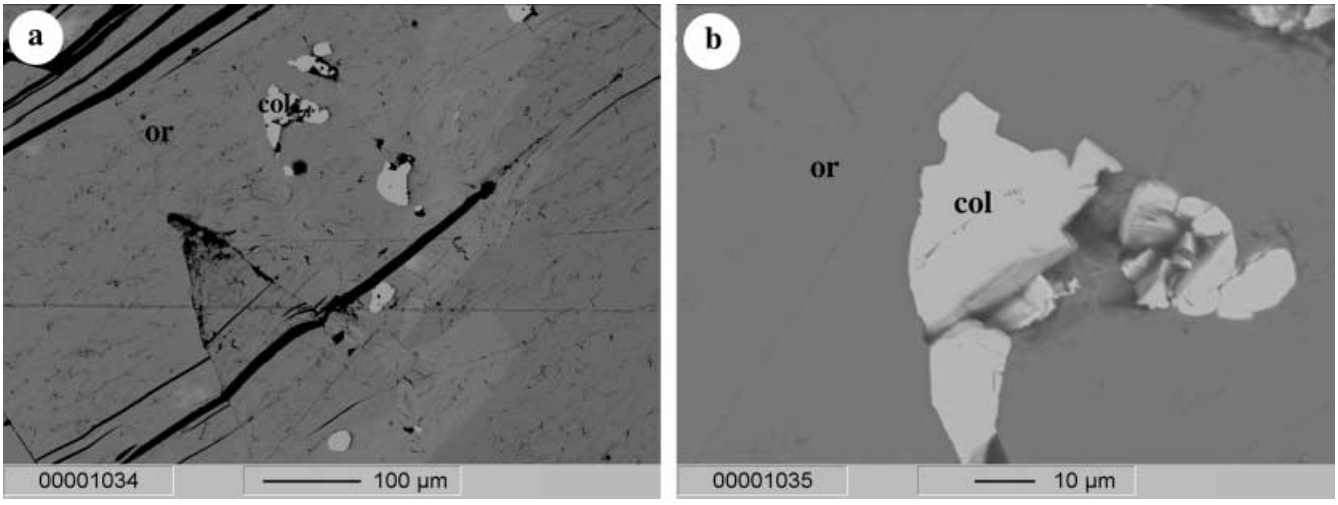

Fig. 13 Back-scattered electron micrographs of coloradoite grains (*col, white*) in orpiment matrix: **a** overview image and **b** detail image. Sample 96119

mineralisation is associated, and a later, pervasive and vein-type silicification with which mineralisation is associated. The unmineralised silicified rocks are white and contain fewer sulphides, and then mainly pyrite, compared to the mineralised rocks. Arsenical pyrite and sphalerite, arsenic–antimony–thallium sulphides, lead-sulphosalts, iron oxides and gangue minerals are commonly present in the mineralised jasperoids. The presence of metallic gold 3–5 µm in size in jasperoids was reported by Karimi (1993), but this has not been confirmed by the present study. Detrital or sedimentary quartz crystals, disseminated in the matrix of unmineralised carbonate rocks, are typically much coarser (0.4 mm) than the hydrothermal quartz.

Argillisation, alteration of feldspars to phyllosilicates and quartz, extends throughout and beyond the zones of gold mineralisation. This alteration is best developed in the granitoid and the Zarshuran black shale where it is pervasive and intimately associated with mineralisation. Intensely argillised black shale comprises fine-grained kaolinite, illite, sericite, quartz, calcite, pyrite, cinnabar and orpiment (samples 96108, 96109, 96116, 97201, 97206). Sericite forms about 50 vol% of the altered granitoid.

Weak mylonitisation generated further fragmentation and caused additional porosity and opened pathways for penetration of air; cool fluids may also have moved downward along these pathways. This air and fluid penetration led to oxidation and acid leaching along fractures and faults. This is manifested by the oxidation of pyrite and other ferruginous sulphides to hematite and goethite (Fig. 14), and by the formation of secondary oxides containing sulphur, iron and arsenic, such as anhydrite, jarosite, scorodite and arsenic oxides. A fracture zone, 5 m wide, affected by oxidation and acid leaching is found to the southeast of Zarshuran, along the Karbelai-Abbas valley. Kuehn and Rose (1992, 1995) attribute similar oxidation and acid leaching in sediment-hosted gold deposits of Nevada to deep weathering, although they are often considered to be hypogene processes, coinciding with the later stages of hydrothermal mineralisation (Radtke 1985).

Some of the accessory minerals in the granitoid at Zarshuran are found in association with hydrothermal alteration and mineralisation. Xenotime (YPO_4) and rutile (TiO_2) are found in altered granitoid (Fig. 15a). Xenotime often contains erbium, cerium and other rare earth elements, as well as thorium, uranium, aluminium, calcium, beryllium, zirconium; it occurs as an accessory mineral in granites and pegmatites (Bate and Jackson 1980). Rutile also occurs as inclusions in the core of zoned pyrite crystals in the black shale (Fig. 15b). Apatite ($CaPO_4$) is found as inclusions in the arsenic-rich rims of zoned pyrites.

Gangue minerals introduced with the mineralisation include barite, fluorite, calcite and dolomite. They occur in minor amounts as single minerals, patches, veins and veinlets in close association with late hydrothermal quartz.

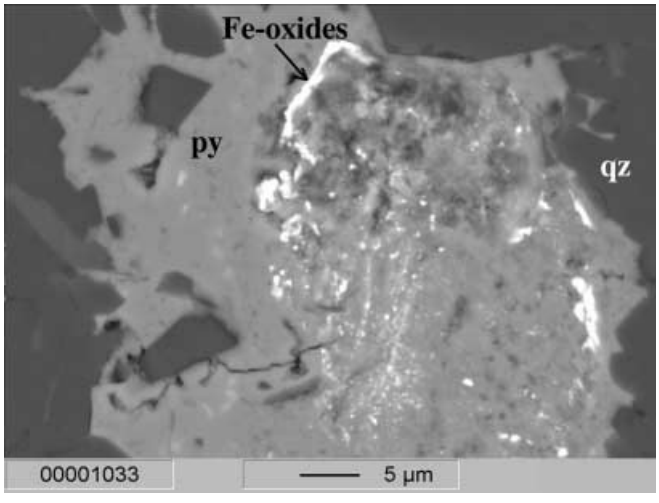

Fig. 14 Back-scattered electron micrograph of gradual oxidation of pyrite to hematite. Sample 97113

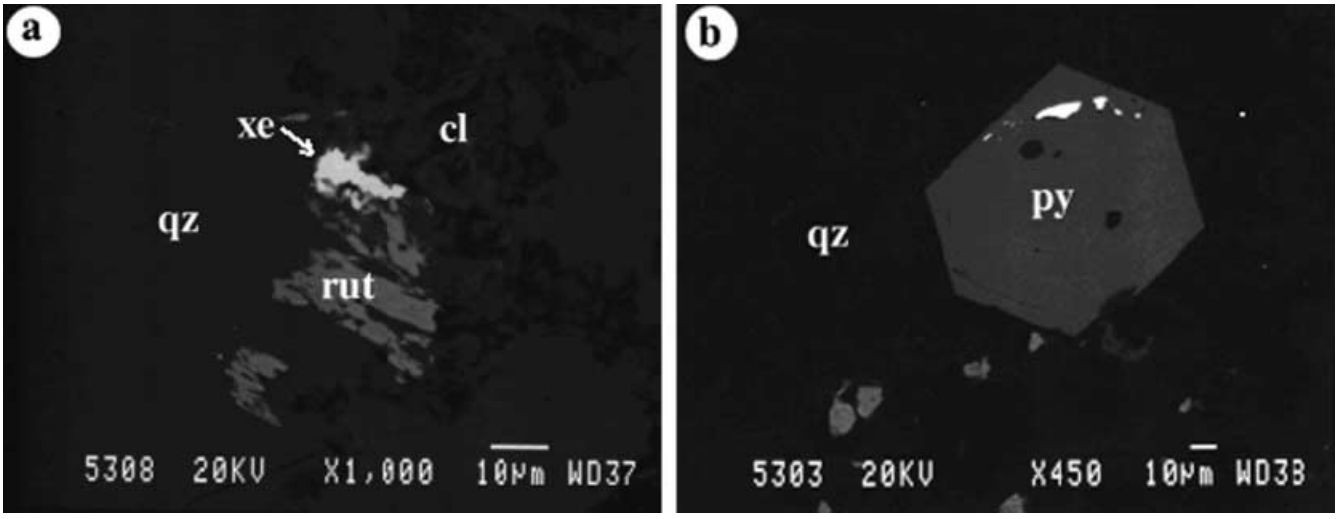

Fig. 15 Back-scattered electron micrographs of accessory minerals: **a** xenotime (*xe, bright*) and rutile (*rut, grey*) associated with clay minerals and quartz; **b** apatite (*ap, bright*) inclusion within the rim of pyrite, and rutile inclusion (*rut, dark grey spot*) in the core of pyrite. Samples 96108, 96114

Paragenetic sequence

Mineral assemblages at Zarshuran include minerals of up to four different origins: primary host rock minerals; minerals formed from primary minerals by replacement due to the hydrothermal solutions; minerals formed by direct crystallisation from hydrothermal solutions; and secondary minerals resulting from weathering of hydrothermal minerals. The paragenetic sequence is complicated by the recognition of three different assemblages related to hydrothermal processes. The mineral assemblages are shown in their inferred paragenetic sequence in Fig. 16.

Primary assemblage

Unaltered rocks are rare and primary minerals are remnants within altered rocks. Those in the sedimentary rocks are detrital quartz (Quartz I), calcite, and diagenetic pyrite (Pyrite I). Both quartz and pyrite occur as anhedral grains along bedding planes in black shale and as framboids disseminated in the matrix of carbonate rocks. Those in the granitoid are quartz, feldspar, zircon, xenotime and rutile.

Early hydrothermal assemblage

This comprises quartz (Quartz II), sericite, illite, kaolinite, pyrite (Pyrite II) and pyrrhotite. In the granitoid the predominant minerals are clays resulting from feldspars alteration whilst the carbonate and black shale are characterised by weak argillic alteration and the introduction of large quantities of silica at the expense of calcite. Pyrrhotite inclusions in this pyrite (Karimi 1993) are interpreted as the earliest sulphide minerals at Zarshuran, precipitating from a hydrothermal solution that contained insufficient sulphur to precipitate pyrite. There is no gold in the minerals of this assemblage.

Main hydrothermal assemblage

In carbonates and black shale, this is marked by the precipitation of a wide range of sulphides and sulphosalts and the continuation of silicification and argillic alteration. The zinc and lead introduced by these fluids precipitated anhedral–euhedral grains of sphalerite (Sphalerite I) and galena. The arsenic formed anhedral–euhedral grains of arsenical pyrite and overgrowths of arsenical pyrite on pre-existing pyrite (Pyrite I and Pyrite II). The arsenical pyrite contains traces of gold, antimony and mercury. Gold also precipitated as micrometre-sized grains of metallic gold, which are found in jasperoids, along with hydrocarbons and gold-bearing arsenical pyrite, and as inclusions in later orpiment. Evolution of the fluid resulted the precipitation of lead-sulphosalts, replacing both sphalerite and arsenical pyrite rims. Still later, the hydrothermal solution, now enriched in antimony, precipitated stibnite. Subsequent depletion of antimony led to precipitation of getchellite, which is often intergrown with stibnite and occurs as open-space fillings in both quartz and calcite (which in places it cross-cuts). The thallium in the fluids then precipitated as christite and lorandite, and the tellurium precipitated as coloradoite. In the granitoid there is weak pyrite (Pyrite II) and cinnabar mineralisation.

Late hydrothermal assemblage

Large quantities of orpiment and realgar were deposited as veins, veinlets, small lenses and open-space fillings. Network and massive arsenical pyrite enclosing arsenical pyrite rims and colloform arsenical pyrite intimately intergrown with massive and colloform sphalerite

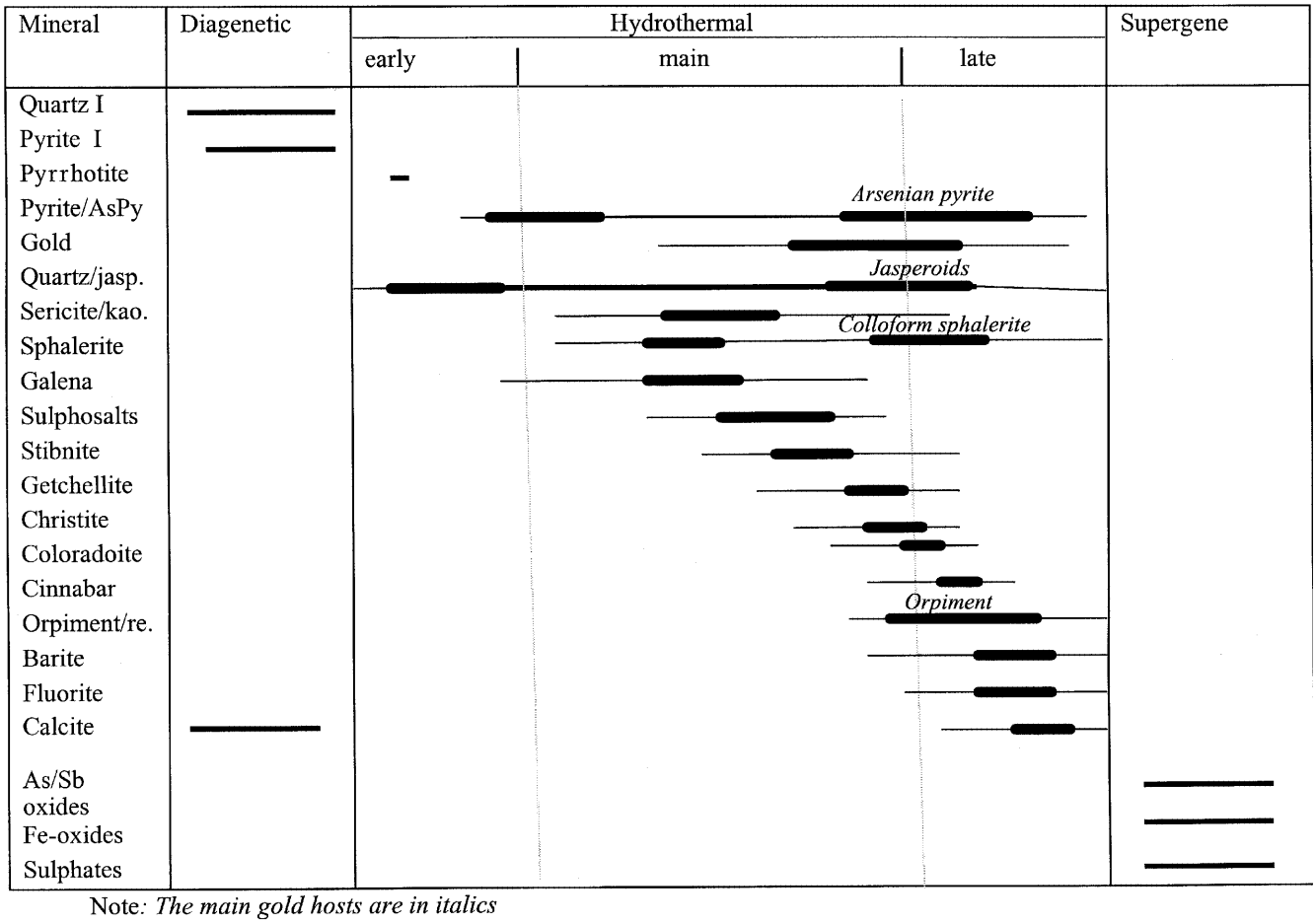

Fig. 16 Paragenetic sequence in the Zarshuran gold deposit

(sphalerite II) were formed in late quartz (Quartz II) veins. The fluids were enriched in gold, resulting in the precipitation of invisible gold in late arsenical pyrite and colloform sphalerite. Barite, quartz (Quartz II), calcite and fluorite were also precipitated, mainly as veins, veinlets and open-space fillings.

Weathering assemblage

Oxidation pyrite, orpiment and stibnite oxidised formed oxides of iron, arsenic and antimony and liberated SO_4^{2-}. This reacted with Ca^{2+}, Fe^{2+}, Ca^{2+}, Ba^{2+} and Al^{3+} to form sulphates.

Discussion

The petrological and mineralogical characteristics of the Carlin-type sediment-hosted disseminated gold deposits of the western United States and southeastern China have been described by Radtke et al. (1972), Wells and Mullens (1973), Bagby and Berger (1985), Radke (1985), Bakken et al. (1989, 1991), Berger and Bagby (1991), Kuehn and Rose (1992) and Arehart et al. (1993). A comparison of the characteristics of the Carlin-type deposits with those of the Zarshuran gold deposit reveals much in common, e.g.

- finely laminated black shale and silicified carbonate host rocks,
- abundant organic matter in host rocks,
- widespread decalcification, silicification and argillisation,
- disseminated mineralisation,
- sulphide minerals with colloform texture occupying open spaces,
- abundance of arsenic minerals, but scarcity of arsenopyrite,
- high concentrations of antimony in orpiment and occurrence of getchellite,
- high concentrations of zinc associated with mineralisation,
- low concentrations of copper associated with mineralisation,
- occurrence of christite, lorandite and lead-sulphosalts,
- association of arsenic, antimony, mercury and thallium with gold,
- rare native gold in orpiment, realgar and silica,
- invisible gold in arsenical pyrite.

On the other hand, Zarshuran has some characteristics that it does not share with the Carlin-type sediment-hosted disseminated gold deposits of the western United States and southeastern China, e.g.

- presence of a mylonitised, highly altered and weakly mineralised granitoid,
- presence of tellurium in arsenic minerals and as coloradoite,
- occurrence of significant amounts of invisible gold in colloform sphalerite.

The mylonitised and weakly mineralised granitoid intrusion at Zarshuran contrasts with the setting of typical sediment-hosted disseminated gold deposits. The unmineralised granitoid contains 140 ppb Au, compared to 80 ppb in the Iman-Khan schist and 70 ppb in the Eocene volcanics located 3 km to the southwest. Its emplacement led to faulting, fracturing and an increase in porosity of the Precambrian formations, in particular the Chaldagh limestone and Zarshuran black shale. As a result, these formations were able to provide channels along which the weakly acid fluid associated with the intrusion invaded the black shale and limestone. According to Radtke (1985) and Berger and Bagby (1991), fluid circulation in the carbonate host formations causes decalcification and further increases porosity and permeability, thus preparing more favourable conditions for mineralisation. Into rocks so prepared at Zarshuran, hydrothermal solutions introduced silica, arsenic, base metals and gold, whilst in the mylonitised granitoid the same solutions effected sericitisation, argillisation and silicifictation and precipitated pyrite and cinnabar. Thus it appears that not only did the intrusion play a role in ground preparation for mineralisation, but also the granitoid and associated magmatic fluids were a source for (part of) the gold-mineralising hydrothermal solutions.

Telluride minerals have not been reported from the sediment-hosted disseminated gold deposits of the western United States and southeastern China. Gold ore from Carlin contains only traces of tellurium (< 0.6 ppm) and no telluride minerals have been found (Radtke 1985). Coloradoite, accompanied by several gold tellurides, was reported by Callow and Worley (1965) from the epithermal volcanic-hosted Acupan gold deposit in the Philippines. The tellurium at Acupan is attributed to a magmatic source (Cooke et al. 1996). Thus the presence of coloradoite and the relatively high tellurium content in arsenic minerals at Zarshuran suggests a magmatic component in the hydrothermal fluids. The absence of gold telluride minerals is attributed to a low tellurium fugacity. According to Chizhikov and Shchastlivyi (1970), coloradoite is the first telluride to be precipitated from a hydrothermal solution of low tellurium fugacity.

The organic matter in the sediment-hosted disseminated gold deposits is derived from the dissolution of carbonate rocks by hydrothermal solutions (Taylor 1986) or an igneous source (Kuehen and Rose 1995). Both possibilities exist at Zarshuran. At Carlin, Radtke (1985) found that the mineralised rocks contain significantly more organic carbon than unmineralised rock; when the organic content of the ore exceeds 0.3 wt%, there is a high gold concentration associated with organic matter, indicating that organic carbon plays an important role in the deposition of gold (Radtke and Scheiner 1970). There is certainly a spatial relation between organic carbon and gold at Zarshuran. Hausen and Park (1986) found that the ores at Getchell and Alligator Ridge contain bituminous matter that was emplaced in the host rocks prior to gold mineralisation and mobilised locally by hydrothermal solutions. Similarly, the Zarshuran black shale represents a source of organic matter that could have been locally mobilised by hydrothermal solutions.

Conclusions

The petrography, mineralogy and trace element geochemistry of the Zarshuran gold deposit show that it is a Carlin-like sediment-hosted disseminated gold deposit. The association of mineralisation at Zarshuran with a magmatic intrusion and the presence of tellurium in concentrations sufficient to precipitate telluride suggest a greater magmatic component in the mineralising hydrothermal solution than is typical for most Carlin-type deposits.

References

Arehart GB, Chryssoulis LS, Kesler SE (1993) Gold and arsenic in iron sulphides from sediment-hosted disseminated gold deposits: implications for depositional processes. Econ Geol 88: 171–185

Asadi HH, Voncken JHL, Hale M (1999) Invisible gold at Zarshuran, Iran. Econ Geol 94: 1367–1374

Bagby WC, Berger BR (1985) Geologic characteristics of sediment-hosted, disseminated precious metal deposits in the western United States. In: Berger BR, Bethke PM (eds) Geology and geochemistry of epithermal systems. Rev Econ Geol 2: 169–202

Bakken BM, Hochella MF, Marshall AF, Turner AM (1989) High resolution microscopy of gold in unoxidized ore from Carlin mine, Nevada. Econ Geol 84: 171–179

Bakken BM, Brigham RH, Fleming AF (1991) The distribution of gold in unoxidized ore from Carlin-type deposits revealed by secondary ion mass spectrometry (SIMS). Geol Soc Am, Annu Meet, Abstr, vol 52, p 228

Bariand P (1962) Contribution à la mineralogie de l'Iran. PhD Thesis, Univ Paris, Faculte des Sciences, Ser A, No 980

Bariand P, Cesborn F, Agrinier H, Geffroy J, Issakhanian V (1968) La Getchellite, $AsSbS_3$, de Zarshuran, Afshar, Iran Bull Soc Fr Mineral Crystal 95: 403–406

Bate RL, Jackson JA (1980) Glossary of geology, 2nd edn. Am Geol Inst, Virginia

Berger BR, Bagby WC (1991) The geology and the origin of the Carlin-type deposit. In: Foster RP (ed) Gold metallogeny and exploration. Blackie, Glasgow, pp 210–248

Callow KJ, Worley BW (1965) The occurrence of telluride minerals at the Acupan gold mine, Mountain province, Philippines. Econ Geol 60: 251–268

Chizhikov DM, Shchastlivyi VP (1970) Tellurium and the tellurides. Collets, London

Cooke DR, Mcphail DC, Bloom MS (1996) Epithermal gold mineralization, Acupan, Baguio district, Philippines: geology, mineralization, alteration and the thermochemical environment of ore deposition. Econ Geol 91: 243–272

Dickson FW, Radtke AS, Geissberg BG, Heropoulos C (1974) Solid solutions of antimony, arsenic and gold in stibnite (Sb_2S_3), orpiment (As_2S_3) and realgar (AsS). Econ Geol 69: 591–594

Glass HJ, Voncken JHL (1996) The Delft Opaque Mineral Identification Program. Mineral Soc Bull 112: 11

Hausen DM, Park WC (1986) Observation on the association of gold mineralization with organic matter in Carlin-type ores. In: Dean WE (ed) Proc Symp Organics and Ore Deposition, Denver Region. Explor Geol Soc, pp 119–136

Karimi M (1993) Geology, petrography, and mineralogical studies of Zarshuran gold deposit (in Persian). Kansaran Engineering Consultant, Tehran

Kuehn CA, Rose AW (1992) Geology and geochemistry of wall-rock alteration at the Carlin gold deposit, Nevada. Econ Geol 87: 1697–1721

Kuehn CA, Rose AW (1995) Carlin gold deposit, Nevada: origin in a deep zone of mixing between normally pressured and over-pressured fluids. Econ Geol 90: 17–36

Kühnel RA, Prins JJ, Roorda HJ (1980) The Delft System for mineral identification. Delft University of Technology, Delft

Mehrabi B, Yardley BWD, Cann JR (1999) Sediment-hosted disseminated gold mineralization at Zarshuran, NW Iran. Miner Deposita 34: 673–696

Oberthur T, Weiser T, Amanor SL (1997) Mineralogical setting and distribution of gold in quartz veins and sulphide ores of the Ashanti mine and other deposits in the Ashanti belt of Ghana: genetic implications. Miner Deposita 32: 2–15

Ojaghi B (1995) Geology of Zarshuran gold deposit (in Persian). Kansaran Engineering Consultant, Tehran

Radtke AS (1985) Geology of the Carlin gold deposit, Nevada. US Geol Surv Prof Pap 1267

Radtke AS, Scheiner BJ (1970) Studies of hydrothermal gold deposition at the Carlin gold deposit, Nevada: the role of carbonaceous materials in gold deposition. Econ Geol 65: 87–102

Radtke AS, Taylor C, Christ CL (1972) Chemical distribution of gold and mercury at the Carlin deposit, Nevada. Geol Soc Am, Annu Meet, Abstr, vol 4, p 632

Radtke AS, Taylor C, Heropoulos C (1973) Antimony-bearing orpiment, Carlin gold deposit, Nevada. J Res US Geol Surv 1: 85–87

Radtke AS, Dickson FW, Slack JF, Brown KL (1977) Christite, a new thallium mineral from the Carlin gold deposit, Nevada. Am Mineral 62: 421–425

Samimi M (1992) Reconnaissance and preliminary exploration in the Zarshuran area (in Persian). Kavoshgaran Engineering Consultant, Tehran

Taylor BE (1986) Magmatic volatiles: isotopic variations of C, H and S. In: Valley JW, Taylor HP, O'Neil JR (eds) Stable isotopes. Mineral Soc Am 16: 185–226

Wells JD, Mullens TE (1973) Gold-bearing arsenian pyrite determined by microprobe analysis, Cortez and Carlin gold mines, Nevada. Econ Geol 68: 187–201